Granular Matter (2019) 21:102
https://doi.org/10.1007/s10035-019-0951-1

ORIGINAL PAPER

Jamming by shear in a dilating granular system

Meimei Wang[1,2] · Dong Wang[2] · Joshua E. S. Socolar[2] · Hu Zheng[2,3,4] · Robert P. Behringer[2]

Received: 12 February 2019 / Published online: 24 September 2019

Abstract
Jamming can occur in frictional granular materials undergoing shear at a fixed packing fraction, ϕ, within a range below the isotropic jamming point, with the amount of strain required to induce jamming, γ, increasing with decreasing ϕ. We are interested in how the shear jamming process is affected when the system dilates as it is sheared. We conduct experiments to shear a 2D granular system while continuously increasing the system volume. Below a certain dilation rate, the system is still able to jam for ϕ smaller than the initial ϕ_0. We measure γ for different dilation rates and initial packing fractions by monitoring the coordination number of non-rattlers and the system pressure. We find that γ is the same as the γ required to jam a system with fixed packing fraction ϕ via pure shear.

Keywords Jamming · Dilating · Granular system · Photoelastic experiment

1 Introduction

Granular materials are among the most commonplace materials in the world, being collections of disordered, solid particles that are ubiquitous in nature and industry [1]. A granular material exhibits a rich set of complex behaviors, including coexistence of gas, fluid and solid phases [1–3]. The transition from fluid-like to solid-like granular states has attracted much scientific attention in recent years [4–6], as the nature of this "jamming" transition is an essential question in a variety of contexts, ranging from foams [7] to glasses [8], from colloids [9] to suspensions [10–12], and from polymer melts [13] to geo-hazards [14, 15].

For a granular system undergoing isotropic compression, the jamming transition happens at a critical packing fraction, ϕ_J [4, 16]. Using photoelastic techniques, the internal force chain network that carries the stresses in the solid phase can be visualized in studies of monolayers of plastic disks [17]. Under compression, an isotropic force network is formed and short range spatial correlations are found in all directions. Jamming, in this situation, is induced by unavoidable formation of contacts between particles as the volume is decreased.

A jamming transition can also occur when a system is subject to pure shear [5]. In this case, the force network in the jammed system is anisotropic, both in the angular distribution of contact forces and in the spatial correlations of force magnitudes. A system usually enters the fragile regime before reaching the fully shear jammed state. In the fragile regime, the force network percolates in only one direction [18], while in the fully shear jammed state it percolates in both directions. The lowest packing fraction at which shear jammed states can form is designated ϕ_S. For higher packing fractions, full shear jamming occurs at sufficiently large shear strains. The transitions between unjammed, fragile, and shear jammed states can be identified through measurements of both the system pressure and the numbers of contacts between particles [19, 20].

In this work, we describe experiments that probe the structure of jammed states formed in a granular system that is dilating while being sheared. We conduct experiments

This article is part of the Topical Collection: In Memoriam of Robert P. Behringer.

✉ Hu Zheng
tjzhenghu@gmail.com

[1] School of Civil and Resource Engineering, University of Science and Technology Beijing, Beijing 100083, China

[2] Department of Physics and Center for Non-linear and Complex Systems, Duke University, Durham, NC 27708, USA

[3] Department of Geotechnical Engineering, College of Civil Engineering, Tongji University, Shanghai 200092, China

[4] School of Earth Science and Engineering, Hohai University, Nanjing 211100, Jiangsu, China

on a layer of photoelastic disks with a novel biaxial experimental apparatus that allows us to independently impose desired shear and dilation rates, while basal friction effects are eliminated by floating the particles in a density matched solution [6]. We deform a rectangular sample of particles into any desired rectangular shape, compressing in one direction while expanding in the other. For different dilation rates, we determine the minimum shear strain required to form fragile or shear jammed states. We find no essential difference in the critical strains associated with different shear-dilating protocols. Furthermore, system pressures (as measured by the G^2 technique [21]), as well as the average coordination numbers of non-rattlers, Z_{NR}, collapses when plotted as a function of the non-rattler fraction, f_{NR}.

2 Experimental techniques

2.1 Experimental apparatus

The 2D biaxial apparatus consists of a horizontal rectangular container. The locations of the four container walls are individually controlled by stepper motors that can move them forward and backward, allowing the imposition of various types of deformation, including pure shear, uniaxial compression and biaxial compression. An illustration of the biaxial setup is shown in Fig. 1a. For a typical pure shear experiment, we compress the system in one direction (moving two opposing walls in the directions of red arrows in Fig. 1a) and dilate it in the other (moving the other two opposing walls in the directions of blue arrows in Fig. 1a) while maintaining a constant total area. The granular system in our experiments consists of bidisperse photoelastic disks (PSM-4 from Vishay Inc.) of diameters $d = 16$ mm and 12.8 mm with a number ratio 1:1, which avoids crystallization of the packing. All disks have the same thickness 6.35 mm, Young's modulus 4 MPa, and friction coefficient $\mu \approx 1.05$. The total number of particles used varies from 890 to 940, resulting in the initial packing fractions ϕ_0 between 77.55 and 81.9%. To initialize each run, we arrange the particles randomly to generate a disordered packing with no inter-particle forces.

As Fig. 1b shows, the particles are floating in a density-matched solution to remove friction between particles and the container base [6]. With a panel LED light source on the bottom, particles under stress will show intensity variations when viewed with crossed circular polarizers: one circular polarizer just above the light panel and the other just below the lens of a high resolution camera (Canon 6D, 5472×3648 pixel^2). The top polarizer can be moved by a stepper motor in and out of the field of view of the camera. The camera records two images at each deformation step, one with and one without the second polarizer. The latter, referred as a normal or unpolarized image, allows us to track the particle positions. The former, referred as a polarized image, shows the photoelastic response of all the particles, revealing particle-scale forces and contacts. The pressure is determined by computing the mean squared gradient of the intensity of the polarized image, $\langle G^2 \rangle$ [21, 22]. Two particles are deemed to be in contact when the distance between these two particles is sufficiently small and $\langle G^2 \rangle$ of the area around the potential contact is reliably determined to be above the noise level.

2.2 Experimental protocol

The protocol for shear with dilation is based on that for pure shear. Starting from an initial packing fraction ϕ_0, we prepare the system with a square "box" of side width $l_0 = 435$ mm. A certain number of disks are placed randomly without contact forces. For the case of pure shear, we compress the system in one direction and dilate it in the other direction, keeping the total area of the box constant. The pure shear strain is defined as $\gamma_0 = \Delta l / l_0$, where Δl is the total displacement in the compression direction. To shear the system with dilation, the dilation step size is chosen to

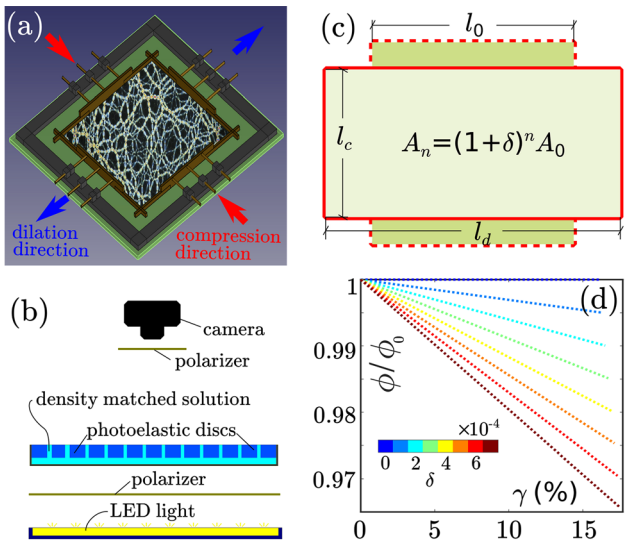

Fig. 1 **a** Schematic of 2D biaxial experimental apparatus. The four boundaries are driven by step motors to generate different protocols. For instance, we compress the system in one direction and dilate in another to shear the system. **b** A vertical view of the optical experiment setups. **c** Sketch of shear with dilation. Where, l_0 is the initial length for each wall and becomes l_c in the compression direction and l_d in the dilation direction, A_0 is the initial area and becomes A_n at step n, δ is the dilation rate. **d** The shear protocol for shear with dilation. ϕ is the real packing fraction at some shear strain, and ϕ_0 is the initial packing fraction. The vertical axis is the ratio between them. The dilation rate varies from 0 to 0.07% indicated by different colors here (color figure online)

be larger than that required for pure shear so that the box area increases after the deformation. To realize a gradually dilating process, we increase the area step by step with a constant expansion ratio. For this type of deformation, shown in Fig. 1c, we first define the dilation rate, δ, which is a constant for each step via the relation $A_n = (1+\delta)^n A_0$, where A_0 and A_n are the box areas at step 0 (i.e. the initial step) and step n, respectively. The total deformation consists of a pure shear $\gamma = 1-(1+\delta)^{(-n/2)} \times (1-\gamma_0)$ coupled with an isotropic expansion characterized by δ.

When $\delta = 0$, the protocol corresponds to pure shear and we have $\gamma = \gamma_0$. The ratio between ϕ at any given γ and the initial value ϕ_0 decreases with γ as shown in Fig. 1d for different choices of δ. The maximum magnitude of shear strain achievable with our apparatus is $\gamma_{max} = 17.55\%$. We have performed experiments at 8 values of δ's between 0 and 0.07%. For each combination of ϕ_0 and δ we collect data from three runs.

3 Results and discussions

3.1 System pressure and coordination number

As shown previously [5, 19], mechanically stable force and contact networks form and evolve during the process of shear jamming. Associated with these force and contact networks are increases of system pressure and coordination number (the average number contacts per particle). We study these quantities for various dilation rates $\delta > 0$ beginning with a given initial packing fraction. Figure 2 shows the results obtained for 8 values of δ and a representative initial packing fraction $\phi_0 = 80.16\%$.

The system pressure can be tracked by computing the average of G^2 over all particles. At the beginning of each run, $\gamma = 0$, we observe a noise level of $\langle G \rangle^2 \sim 0.26$. $\langle G \rangle^2$ starts to increase rapidly after γ reaches a threshold value for each run, as shown in Fig. 2a. The value of γ where $\langle G^2 \rangle$ starts to increase appears to depend on δ and will be discussed further in Sect. 3.2. The subsequent behavior of $\langle G^2 \rangle$ as a function of γ depends on δ. For small $\delta < 0.03\%$, $\langle G^2 \rangle$ increases monotonically with γ, as seen in the blue and cyan curves in Fig. 2a, until particles undergo out-of-plane buckling, at which point the run is terminated. For $\delta > 0.05\%$, on the other hand, $\langle G^2 \rangle$ first increases with γ, then decreases, as seen in the red curves in Fig. 2a. The latter behavior may be expected for all δ if buckling could be avoided; at sufficiently high dilations, the packing cannot be jammed (unless the packing fraction becomes strongly inhomogeneous).

Next we consider some properties of the evolving contact networks as a function of shear strain γ. We measure Z_{NR}, the average coordination number per particle excluding rattlers; i.e., excluding the contributions from particles that have fewer than two contacts. Our definition of Z_{NR} counts all of the contacts of the remaining particles, including contacts with the excluded particles. This definition is motivated by experimental considerations. Contacts are identified by detecting photoelastic responses indicative of contact forces [17]. Because the particles are floating in a solution, there are no basal friction forces, and any particle that is bearing force should always have more than one contact. Rattlers are typically particles with no identified contacts. However, there may be a few particles with only one contact with an apparent force strong enough to be detected by our algorithm, which may be either a false positive or be due to the presence of other contacts that were not detected. We note that the theoretical value of this measured Z_{NR} at the shear jamming transition is not precisely known due both to the experimental detection threshold and to the possibility of having portions of the stress network that are not truly rigid [23]. Nevertheless, the criterion $Z_{NR} = 3$ is expected to be close to the true value for the isostatic packings and appears to correspond well with the onset of a change in behavior of $\langle G^2 \rangle$.

The relationship between Z_{NR} and γ (Fig. 2b) shows a behavior similar to that of $\langle G^2 \rangle$. Given our definition of

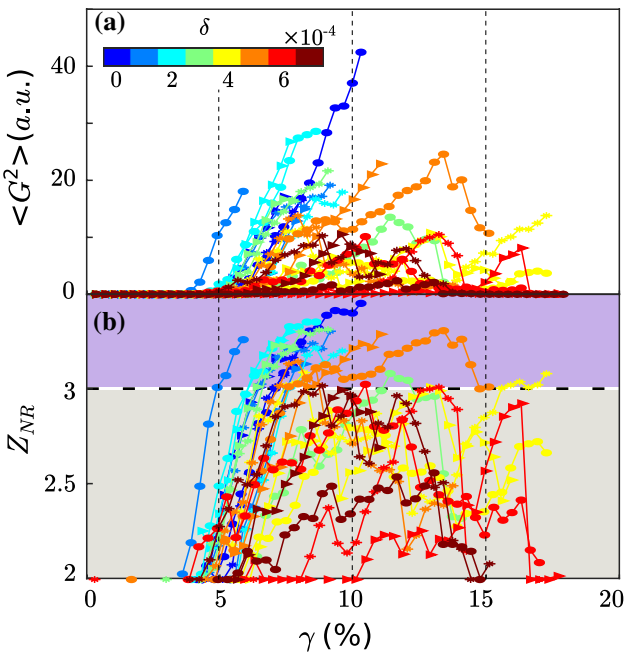

Fig. 2 **a** $\langle G^2 \rangle$ versus shear strain γ for different dilation rates with initial packing fraction of 80.16%. $\langle G^2 \rangle$ is proportional to the system pressure. The dilation rate increases from 0 to 0.07% per step. Here, we include three sets of experiments for each dilation rate, marked as dots, triangles and stars. **b** The mean contact number of the non-rattlers Z_{NR} versus shear strain γ for the same set of data. The granular system is jammed when $Z_{NR} \geq 3$, which is shown as the purple region. The gray region is corresponding to unjamming state, while $Z_{NR} \leq 3$ (color figure online)

Z_{NR}, its minimum value is 2, which occurs for our initial unjammed packings. From there, Z_{NR} increases with γ and either terminates due to out-of-plane buckling of particles or reaches a peak and then decreases. Note that when considering the numbers of constraints associated with each contact, all the contacts detected in our experiments should be considered to be static rather than sliding [23]. Any sliding contact will either disappear or convert to a static one because of the absence of basal friction and the long waiting time (more than 10 s) at each strain step. We define the jamming transition as occurring when Z_{NR} reaches 3, which is the minimum coordination number required for mechanical stability in an isostatic 2D frictional system [5, 24]. The data for $\langle G^2 \rangle$ and Z_{NR} clearly show a transition from a stress-free, fluid-like state to a rigid state, indicating that shear induced jamming does happen in a frictional granular system that is dilating.

The relationship between $\langle G^2 \rangle$ (or Z_{NR}) and γ shows a clear dependence on ϕ_0 and δ. However, it has been shown that f_{NR}, the fraction of particles that are not rattlers, is a better control parameter than γ in determining properties of force networks [5, 19, 25]. If we plot here all the data for $\langle G^2 \rangle$ or Z_{NR} from runs with various ϕ_0 and δ as a function of f_{NR} rather than γ, they collapse well into a single curve, as shown in Fig. 3. (Because the relation between Z_{NR} and f_{NR} is monotonic and almost linear here, plots of f_{NR} vs γ would look quite similar to the plots of Z_{NR} vs γ in Fig. 2.) $\langle G^2 \rangle$ increases slowly when f_{NR} is small ($f_{NR} < 0.6$) and appears to grow rapidly at large f_{NR} ($f_{NR} > 0.6$), and Z_{NR} increases steadily with f_{NR}. We find that $Z_{NR} \approx 3$ occurs for $f_{NR} \approx 0.83$, which is consistent with previous results [5, 19]. The collapse of $\langle G^2 \rangle$ or Z_{NR} data by f_{NR} strongly suggests that the geometry of the contact and force network induced at jamming by shear with dilation is independent of path taken in the space of pure shears and dilation to arrive at the jamming transition.

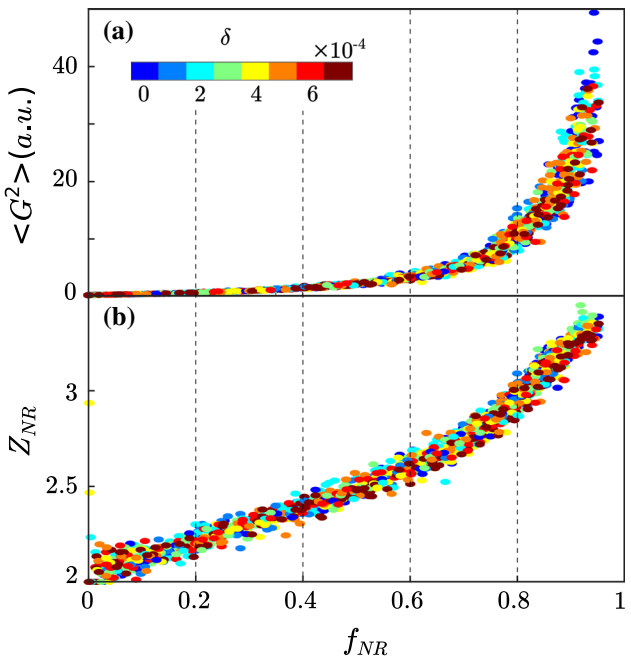

Fig. 3 Data for $\langle G^2 \rangle$ of the system and mean contact number Z_{NR}, versus f_{NR}, for different dilation rates and different initial packing fractions. For either $\langle G^2 \rangle$ or Z_{NR}, all data points collapse onto one single curve, respectively. **a** $\langle G^2 \rangle$ versus f_{NR}, with a jamming phase transition at $f_{NR} \approx 0.83$ (see text). **b** The mean contact number Z_{NR} versus f_{NR} for the same set of data. The jamming transition point corresponds to $Z \approx 3.0$

3.2 Critical shear strain to jam the system

The above results on $\langle G^2 \rangle$ and Z_{NR} establish the existence of shear induced jamming even in a system with $\delta > 0$. We now focus more precisely on how the dilation rate affects the transition. Figure 4 shows the minimum strains needed to reach fragile and shear jammed states, γ_F and γ_{SJ} respectively, as a function of the actual packing fraction, ϕ. γ_F is defined as the shear strain at which $\langle G^2 \rangle$ starts to grow. The system is determined to become fragile when the difference of $\langle G^2 \rangle$ between two consecutive

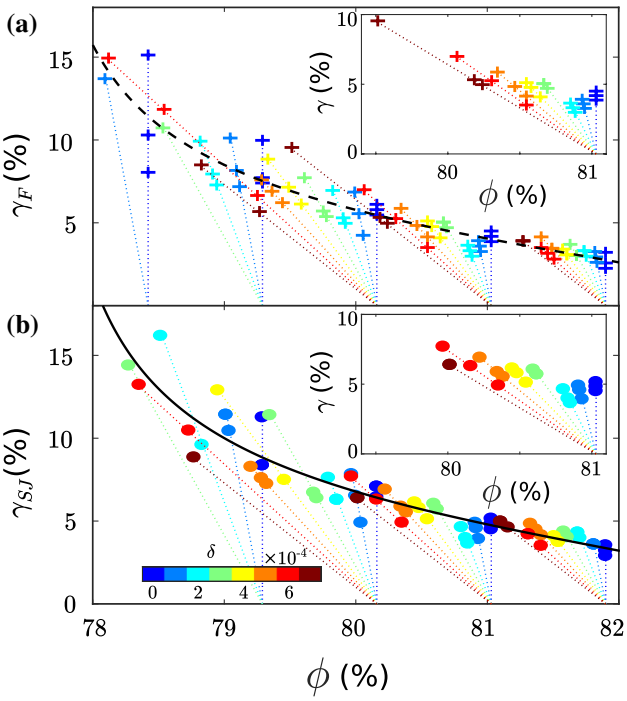

Fig. 4 **a** Phase boundary γ_F, which is extracted from the $\langle G^2 \rangle$ data. The γ_F for different initial packing fraction and dilation rate is fitted by Eq. 3 as the dash dot line. Inset: zoomed-in part of the data points with an initial packing fraction of 81.03%. **b** Phase boundary γ_F, which comes from the Z_{NR} data. The γ_{SJ} for different initial packing fraction and dilation rate is fitted by Eq. 3 as the solid line. Inset: zoomed-in part of the data points with an initial packing fraction of 81.03%. Different colored lines in (**a**) and (**b**) indicate different paths from certain initial packing fraction with different dilation rates, which are indicated by the color map in (**b**) (color figure online)

deformation steps first exceeds a certain threshold, which we choose to be $\Delta = 0.5$ in the arbitrary units used in Fig. 3. γ_{SJ} is the strain at which the coordination number just crosses $Z_{NR} = Z_{iso}$, where Z_{iso} is the coordination number at isotropic jamming, taken here to be 3, as discussed in Sect. 3.1. These criteria can be expressed as

$$\gamma_F(\phi) = \min\{\gamma(\langle G^2\rangle_n - \langle G^2\rangle_{n-1} \geq \Delta;\phi)\}; \quad (1)$$

$$\gamma_{SJ}(\phi) = \min\{\gamma(Z_n \geq Z_{iso};\phi)\}, \quad (2)$$

where $\langle G^2\rangle_n$ is $\langle G^2\rangle$ at the n-th step of deformation.

Figure 4 shows γ_F and γ_{SJ} as functions of ϕ for runs beginning with different ϕ_0's and various values of δ. For each ϕ_0, data were collected from three independent runs. Colored plus signs represent γ_F and colored dots represent γ_{SJ}. Due to the limited maximum γ allowed by the apparatus, the lowest ϕ_0 for which γ_F and γ_{SJ} can be reached is approximately 78.4%. For each ϕ_0 tested, results for different δ are shown in different colors, with dashed lines drawn as guides to the eye showing γ as a function of ϕ for the given run. The inset in Fig. 4 shows all of the data for the specific choice $\phi_0 = 81.03\%$. Clearly, both γ_F and γ_{SJ} increase with δ.

It appears that γ_F and γ_{SJ} depend only on ϕ; they do not depend on the path taken in the γ-ϕ plane to reach jamming. We can fit all the data with a function of the following form:

$$\gamma_X = \gamma_X^C \sqrt{\frac{\phi_J - \phi}{\phi - \phi_S}}, \quad (3)$$

where X may be F or SJ. We find for the fragile phase boundary $\phi_J = 83.1 \pm 0.7\%$, $\phi_S = 77.4 \pm 0.3\%$, and $\gamma_F^C = 5.2 \pm 1.0\%$; and for the jamming phase boundary $\phi_J = 83.4 \pm 1.0\%$, $\phi_S = 77.5 \pm 0.3\%$, and $\gamma_{SJ}^C = 5.8 \pm 1.2\%$. These fits are shown in Fig. 4, by the black solid line for γ_{SJ} and the black dashed line for γ_F. We also fit the data with formula (7) in Ref. [26], which shows exactly the same trend—in the range of data available—but differs functionally/asymptotically in the limits outside our data-range. The consistency of the fits with data from different dilation rates indicate that the actual packing fraction, rather than the initial packing fraction, controls the shear strain needed to transit from unjammed to fragile states, or from fragile to shear jammed states. While higher dilation rates do delay the transitions from a given initial state, they appear to be consistent with a single phase boundary curve in ϕ-γ plane for each transition.

4 Conclusions

We have experimentally studied a 2D granular system under a type of deformation combining pure shear and dilation, referred as shear with dilation. Jamming of the granular system still occurs under this type of deformation for a finite range of packing fractions below the isotropic jamming point. For small dilation rates δ, the system pressure, $\langle G^2\rangle$, and coordination number, Z_{NR}, increase with γ, and when the system pressure is high enough the particles tend to buckle out of the plane. For large δ, the system may never jam or may pass through a jammed phase and later relax back to an unjammed state. Our results suggest that the onset shear strains needed for passing from unjammed to fragile states or from fragile to jammed states depend only on the current packing fraction, regardless of the dilation rate, which we interpret to mean that the structure of the shear jammed state does not depend on the manner in which the jamming transition is approached. Finally, we find that plots of $\langle G^2\rangle$ (or Z_{NR}) as a function of non-rattler fraction collapse onto a single curve for all initial packing fractions and dilation rates tested.

Acknowledgements This work is dedicated to Bob Behringer, whom we are deeply indebted to and will forever miss. His role in supporting and mentoring this research clearly justifies inclusion as a coauthor. Discussions with Aghil Abed Zadeh, Cacey Stevens Bester, Ryan Kozlowski, Yiqiu Zhao and Yuchen Zhao are highly appreciated. This work was funded by NSFC Grant No. 41672256(HZ), NSF Grant Nos. DMR1206351 and DMR1809762, ARO No. W911NF-18-1-0184, NASA Grant No. NNX15AD38G, the William M. Keck Foundation, RT-MRSEC fellowship (DW). MW was supported by the China Scholarship Council.

Compliance with ethical standards

Conflict of interest The authors declare that they have no conflict of interest.

References

1. Jaeger, H.M., Nagel, S.R., Behringer, R.P.: Granular solids, liquids, and gases. Rev. Modern Phys. **68**(4), 1259 (1996)
2. Henkes, S., Chakraborty, B.: Jamming as a critical phenomenon: a field theory of zero-temperature grain packings. Phys. Rev. Lett. **95**(19), 198002 (2005)
3. Behringer, R.P., Chakraborty, B.: The physics of jamming for granular materials: a review. Rep. Progress Phys. **82**(1), 012601 (2018)
4. O'Hern, C.S., Silbert, L.E., Liu, A.J., Nagel, S.R.: Jamming at zero temperature and zero applied stress: the epitome of disorder. Phys. Rev. E **68**(1), 011306 (2003)
5. Bi, D., Zhang, J., Chakraborty, B., Behringer, R.P.: Jamming by shear. Nature **480**(7377), 355 (2011)
6. Zheng, H., Dijksman, J.A., Behringer, R.P.: Shear jamming in granular experiments without basal friction. EPL (Europhys. Lett.) **107**(3), 34005 (2014)
7. Katgert, G., Tighe, B.P., van Hecke, M.: The jamming perspective on wet foams. Soft Matter **9**(41), 9739–9746 (2013)
8. O'Hern, C.S., Langer, S.A., Liu, A.J., Nagel, S.R.: Force distributions near jamming and glass transitions. Phys. Rev. Lett. **86**(1), 111 (2001)

9. Stratford, K., Adhikari, R., Pagonabarraga, I., Desplat, J.-C., Cates, M.E.: Colloidal jamming at interfaces: a route to fluid-bicontinuous gels. Science **309**(5744), 2198–2201 (2005)
10. Peters, I.R., Majumdar, S., Jaeger, H.M.: Direct observation of dynamic shear jamming in dense suspensions. Nature **532**(7598), 214 (2016)
11. Lim, M.X., Barés, J., Zheng, H., Behringer, R.P.: Force and mass dynamics in non-newtonian suspensions. Phys. Rev. Lett. **119**, 184501 (2017)
12. Chen, D.Z., Zheng, H., Wang, D., Behringer, R.P.: Discontinuous rate-stiffening in a granular composite modeled after cornstarch and water. Nat. Commun. **10**(1), 1283 (2019)
13. Rottler, J., Robbins, M.O.: Jamming under tension in polymer crazes. Phys. Rev. Lett. **89**(19), 195501 (2002)
14. Huang, Y., Zhang, W., Qiang, X., Xie, P., Hao, L.: Run-out analysis of flow-like landslides triggered by the ms 8.0 2008 Wenchuan earthquake using smoothed particle hydrodynamics. Landslides **9**(2), 275–283 (2012)
15. Huang, Y., Cheng, H.: A simplified analytical model for run-out prediction of flow slides in municipal solid waste landfills. Landslides **14**(1), 99–107 (2017)
16. Liu, A.J., Nagel, S.R.: Nonlinear dynamics: jamming is not just cool any more. Nature **396**(6706), 21 (1998)
17. Majmudar, T.S., Behringer, R.P.: Contact force measurements and stress-induced anisotropy in granular materials. Nature **435**(7045), 1079 (2005)
18. Cates, M.E., Wittmer, J.P., Bouchaud, J.-P., Claudin, P.: Jamming, force chains, and fragile matter. Phys. Rev. Lett. **81**(9), 1841 (1998)
19. Ren, J., Dijksman, J.A., Behringer, R.P.: Reynolds pressure and relaxation in a sheared granular system. Phys. Rev. Lett. **110**(1), 018302 (2013)
20. Majmudar, T.S., Sperl, M., Luding, S., Behringer, R.P.: Jamming transition in granular systems. Phys. Rev. Lett. **98**(5), 058001 (2007)
21. Howell, D., Behringer, R.P., Veje, C.: Stress fluctuations in a 2D granular couette experiment: a continuous transition. Phys. Rev. Lett. **82**(26), 5241 (1999)
22. Yiqiu Zhao, H., Zheng, D.W., Wang, M., Behringer, R.P.: Particle scale force sensor based on intensity gradient method in granular photoelastic experiments. New J. Phys. **21**(2), 023009 (2019)
23. Henkes, S., Quint, D.A., Fily, Y., Schwarz, J.M.: Rigid cluster decomposition reveals criticality in frictional jamming. Phys. Rev. Lett. **116**, 028301 (2016)
24. Wang, D., Ren, J., Dijksman, J.A., Zheng, H., Behringer, R.P.: Microscopic origins of shear jamming for 2D frictional grains. Phys. Rev. Lett. **120**, 208004 (2018)
25. Ren, J.: Nonlinear dynamics and network properties in granular materials under shear. Ph.D. thesis, Duke University (2013)
26. Kumar, N., Luding, S.: Memory of jamming-mutiscale models for soft and granular matter. Granular Matter **18**(2), 58 (2016)